

Unsupervised Embedding Quality Evaluation

Anton Tsitsulin¹ Marina Munkhoeva² Bryan Perozzi¹

Abstract

Unsupervised learning has recently significantly gained in popularity, especially with deep learning-based approaches. Despite numerous successes and approaching supervised-level performance on a variety of academic benchmarks, it is still hard to train and evaluate SSL models in practice due to the unsupervised nature of the problem. Even with networks trained in a supervised fashion, it is often unclear whether they will perform well when transferred to another domain.

Past works are generally limited to assessing the amount of information contained in embeddings, which is most relevant for self-supervised learning of deep neural networks. This work chooses to follow a different approach: can we quantify how easy it is to linearly separate the data in a stable way? We survey the literature and uncover three methods that could be potentially used for evaluating quality of representations. We also introduce one novel method based on recent advances in understanding the high-dimensional geometric structure of self-supervised learning.

We conduct extensive experiments and study the properties of these metrics and ones introduced in the previous work. Our results suggest that while there is no free lunch, there are metrics that can robustly estimate embedding quality in an unsupervised way.

1. Introduction

With proliferation of unsupervised and self-supervised deep learning methods in the recent years, there is an increasing need to quantify the quality of representations produced by such methods. Across different domains, this is com-

monly done with training linear classifiers (*probes*) against known labels (Perozzi et al., 2014; Chen et al., 2020). However, in unsupervised settings there are no labels to begin with. How can we do model selection, optimize methods' hyperparameters, or even verify the method worked at all?

In search of such metrics, we turn our attention to different sub-fields of numerical linear algebra, machine learning and optimization, and high-dimensional probability. We identify three promising candidate metrics and introduce one based on the expected distribution of embedding distances. We then proceed to test them on two conceptually novel domains: supervised model selection and shallow single-layer graph embedding learning.

Our experimental results indicate there is no “free lunch”—a metric that is universally dominating—thus calling for a comprehensive suite of evaluation metrics. Despite that, metrics introduced in this work exhibit, like stable rank and coherence, display stronger correlation to downstream task performance of the supervised models, are more computationally stable, and suit shallow embedding models much better than state-of-the-art ones.

We summarize our key contributions as follows:

- We identify three different perspectives on evaluation of embedding quality in unsupervised manner and introduce four metrics based on these perspectives.
- We experimentally study two novel settings for embedding quality evaluation, showing that standard metrics often fail when shallow models are being studied.
- We conduct a study on computational stability of all metrics and identify the minimum viable sample sizes.
- We demonstrate that the proposed metrics are at least as effective as state-of-the-art ones in terms of downstream quality prediction while having more intuitive behavior for shallow embedding models.

2. Related Work

The literature on evaluating representations in unsupervised way is still sparse. Arguably, *dimensional collapse* (Hua et al., 2021) has sparked initial interest in the area. In dimensional collapse, some dimensions become non-meaningful (collapse) during training. Because of that problem, three concurrent metrics, which we introduce below, all study the problem of measuring such collapse from different angles.

¹Google Research, New York, USA ²Max Planck Institute for Intelligent Systems, Tübingen, Germany. Correspondence to: Anton Tsitsulin <tsitsulin@google.com>.

α -ReQ (Agrawal et al., 2022) fits a power-law to the singular values of representations, meaning $\lambda_i \propto i^{-\alpha}$. Logarithmic decay of the spectrum with slope $\alpha = 1$ was recently proven to provide the best generalization in infinite-dimensional analysis of linear regression (Bartlett et al., 2020). In practice, a simple linear regression estimator on a log-log scale is used to estimate the value of α . This approach for estimating the power-law exponent is considered inaccurate (Clauset et al., 2009).

RankMe (Garrido et al., 2022; Roy & Vetterli, 2007) is a method based on estimating the effective rank of a matrix. In a strict numerical linear algebraic sense, most embedding matrices are full-rank. “Softer” definitions allow to capture not only fully collapsed dimensions but also general underutilization of the parameter space.

Definition 2.1. Given a matrix $M \in \mathbb{R}^{n_1 \times n_2}$ with SVD $M = U\Sigma V^\top$, its effective rank is the entropy of its normalized singular values, defined as

$$\text{RankMe}(M) = - \sum_i p_i \log p_i, \quad p_i = \frac{\sigma_i}{\|\Sigma\|_1}.$$

NESum (He & Ozay, 2022) analyzes eigenspectrum of the covariance matrix of representations. It is introduced as a heuristic metric complementing the analysis of features learned by the barlow twins loss (Zbontar et al., 2021).

Definition 2.2. Given a matrix $M \in \mathbb{R}^{n_1 \times n_2}$ with covariance that can be decomposed as $C = U\Lambda U^\top$:

$$\text{NESum}(M) = \sum_i \frac{\lambda_i}{\lambda_0},$$

with convention of $\frac{0}{0} = 0$.

3. Three Perspectives on Embedding Quality

We now study three different perspectives on estimating embedding “quality”. All measures we have discussed so far aim to answer an information-theoretic question on representations: *Do embedding carry as much information as their size allows?* However, there are different questions worth answering. This paper introduces four novel metrics for embedding quality evaluation based on different perspectives on the embedding quality.

The following section pursues the linear classifier perspective on representation quality (Mohri & Talwalkar, 2011). It asks: *How hard it is to find a suitable transformation from the representations to the targets of the downstream task?* We show that this is an inherent property of the representations themselves (and the target matrix too, if it’s not a classification task).

3.1. Linear Classifier Perspective

Let our downstream task be a classification with a target matrix $Y \in \{0, 1\}^{n \times c}$ and a linear probe $h = XW + b$ with weight matrix W and bias vector b . In what follows, we argue that it is easier to find h that yields high accuracy when applied to the input matrix X with higher coherence.

Without loss of generality, we can drop the bias term. For the ease of exposition, we will adopt the Mean-Squared Error loss ($\mathcal{L} = \|Y - XW\|_F^2$) for a downstream task. The optimal weight matrix will then depend on the target and representation matrices, i.e. from the derivative condition $X^\top Y = X^\top XW$. Given some $A \in \ker(X)$, i.e. a matrix comprised of vectors from the null space of X , we rewrite the condition as $X^\top Y = X^\top (A + X^\dagger Y)$ and get $W^* = X^\dagger Y + A$ for any $A \in \ker(X)$.

Assuming we can always find an optimal weight matrix, to minimize the loss \mathcal{L} , the representations X should be aligned with the target matrix Y , i.e. the left singular vectors U of $X = U\Sigma V^\top$ should span U_Y of $Y = U_Y \Sigma_Y V_Y^\top$, where $V_Y = I_c$ when Y is a classification target matrix.

Plugging in the optimal W^* into the loss,

$$\begin{aligned} \|Y - X(X^\dagger Y + A)\|_F^2 &= \|Y - U\Sigma\Sigma^\dagger U^\top Y\|_F^2 \\ &= \|(I - U I_d U^\top) Y\|_F^2 \\ &= \|(I - I_d) U^\top Y\|_F^2 \\ &= \|Y\|_F^2 - \|U_d^\top U_Y \Sigma_Y\|_F^2, \end{aligned}$$

where $I_d \in \mathbb{R}^{n \times n}$ with d ones on the diagonal, and the minimum is reached whenever columns in U are aligned with columns in U_Y .

Intuitively, if the representation dimensionality is larger than number of classes in the downstream task, i.e. $d > c$, and X has full rank (a consequence of most methods being spectral embedding), then the representation basis covers the target basis with high probability. However, to quantify the extent of this coverage, we will need to introduce a notion of incoherence.

Definition 3.1 (μ_0 -incoherence). Given matrix $M \in \mathbb{R}^{n_1 \times n_2}$ with rank- r and SVD $M = U\Sigma V^\top$, M is said to satisfy the standard incoherence condition with parameter μ_0 if

$$\max_{1 \leq i \leq n_1} \|U^\top e_i\|_2 \leq \sqrt{\frac{\mu_0 r}{n_1}}, \quad \max_{1 \leq j \leq n_2} \|V^\top e_j\|_2 \leq \sqrt{\frac{\mu_0 r}{n_2}},$$

where e_i is the i -th standard basis vector of a respective dimension. Note that $1 \leq \mu_0 \leq \max(n_1, n_2)/r$.

Informally, standard incoherence characterizes the extent of alignment of the singular vectors to the standard basis.

Incoherence is typically used in low-rank matrix completion problems to estimate a complexity of matrix recovery (Mohri & Talwalkar, 2011). In our setting, lower incoherence will be indicative of high alignment with target matrix and, thus, better performance.

Ideally, if we had access to the targets, we could use joint incoherence $\mu_1(\mathbf{Z}, \mathbf{Y})$ to measure the alignment directly. More practical is the case when true labels are not available. There, we will need to rely on the standard coherence $\mu_0(\mathbf{Z})$ which measures alignment to the standard basis. Our experiments show that there is indeed a correlation between standard incoherence of the representations and performance on the downstream tasks (almost perfect in some cases).

3.2. Numerical Linear Algebra Perspective

Numerical linear algebra provides us with more tools for analysing behaviors of linear classifiers. One of the classic ones is the condition number, or, in the case of non-square matrices, its generalized version (Ben-Israel, 1966). For example, κ_2 is used to detect multicollinearity in linear and logistic regression (Belsley et al., 2005).

Definition 3.2. Pseudo-condition number of a matrix \mathbf{M} with SVD $\mathbf{M} = \mathbf{U}\mathbf{\Sigma}\mathbf{V}^\top$ is defined as

$$\kappa_p(\mathbf{M}) = \|\mathbf{M}\|_p \|\mathbf{M}^\dagger\|_p \stackrel{p=2}{=} \frac{\sigma_1}{\sigma_n}.$$

We are particularly interested in κ_2 , since it is easily computable with SVD, as the pseudo-inverse of \mathbf{M} is $(\mathbf{M}^\top \mathbf{M})^{-1} \mathbf{M} = \mathbf{U} \mathbf{\Sigma}^{-1} \mathbf{V}^\top$, meaning $\|\mathbf{M}^\dagger\|_2 = 1/\sigma_n$.

In the analysis of linear regression, κ_2 can be used to bound the sensitivity of the system to the change in the input. Consider a linear system $(\mathbf{A} + \Delta \mathbf{A})\hat{\mathbf{x}} = \mathbf{b}$ and its perturbed version $\mathbf{A}\hat{\mathbf{x}} = \mathbf{b} + \Delta \mathbf{b}$. Then,

$$\frac{\|\hat{\mathbf{x}} - \mathbf{x}\|}{\|\mathbf{x}\|} \leq \frac{\kappa(\mathbf{A})}{1 - \kappa(\mathbf{A}) \frac{\|\Delta \mathbf{A}\|}{\|\mathbf{A}\|}} \left(\frac{\|\Delta \mathbf{A}\|}{\|\mathbf{A}\|} + \frac{\|\Delta \mathbf{b}\|}{\|\mathbf{b}\|} \right).$$

We use κ_2 to measure stability of learned representations.

3.2.1. STABLE RANK

Stable rank (also called *effective rank* or *intrinsic dimension of a matrix*) is another fundamental quality in numerical analysis of random matrices.

Definition 3.3. Numerical rank of a matrix \mathbf{M} is defined as

$$r(\mathbf{M}) = \frac{\|\mathbf{M}\|_F}{\|\mathbf{M}\|_2}$$

Note that $r(\mathbf{M}) \leq \text{rank}(\mathbf{M})$, and that bound is sharp. Stable rank is a useful tool that guides fundamental numerical problems, including matrix sampling and covariance estimation.

Let us restate Theorem 1.1 from Rudelson & Vershynin (2007):

Theorem 3.4. Let \mathbf{A} be an $n \times d$ matrix with stable rank r . Let $\varepsilon, \delta \in (0, 1)$, and let $m \leq n$ be an integer such that

$$m \geq C \left(\frac{r}{\varepsilon^4 \delta} \right) \log \left(\frac{r}{\varepsilon^4 \delta} \right).$$

Consider a $m \times d$ matrix $\tilde{\mathbf{A}}$, which consists of m normalized rows of \mathbf{A} picked independently with replacement, with probabilities proportional to the squares of their Euclidean lengths. Then with probability at least $1 - 2\exp(-c/\delta)$ the following holds. For a positive integer k , let \mathbf{P}_k be the orthogonal projection onto the top k left singular vectors of $\tilde{\mathbf{A}}$. Then,

$$\|\mathbf{A} - \mathbf{A}\mathbf{P}_k\| = \sigma_{k+1}(\mathbf{A}) + \varepsilon \|\mathbf{A}\|_2.$$

This suggests that the numerical rank determines how hard it is to estimate the matrix by subsampling its rows. Intuitively, a well-distributed representations should be hard to estimate; we will observe that this is indeed the case in practice.

3.3. High-dimensional Probability Perspective

In self-supervised learning, Assran et al. (2023) shows that several contrastive learning methods try to distribute representations equally in the space. High-dimensional probability can provide us with an estimate of pairwise distances when embeddings are distributed uniformly on a d -dimensional unit sphere \mathbb{S}^d .

Given L_2 normalized embeddings $\mathbf{W} \in \mathbb{R}^{n \times d}$, a measure of clustering can be defined using the norm of the pairwise dot product matrix $\mathbf{Q} = \|\mathbf{W}\mathbf{W}^\top\|_F$. Since the expected dot product of high-dimensional isotropic random vectors $\langle \mathbf{x}, \mathbf{y} \rangle \asymp \frac{1}{n}$ (Vershynin, 2018, Remark 3.2.5), we can estimate $\mathbb{E}[\mathbf{Q}] = n + \frac{n(n-1)}{d}$. The maximum metric value $\mathbf{Q} = n^2$ can only be achieved in the collapsed case. Combining all normalizations to get a metric upper-bounded that is upper-bounded by 1, we get:

Definition 3.5.

$$\begin{aligned} \text{SelfCluster}(\mathbf{W}) &= \frac{\|\mathbf{W}\mathbf{W}^\top\|_F - n - \frac{n*(n-1)}{d}}{n^2 - n - \frac{n*(n-1)}{d}} \\ &= \frac{d\|\mathbf{W}\mathbf{W}^\top\|_F - n(d + n - 1)}{(d - 1)(n - 1)n}. \end{aligned}$$

SelfCluster allows us to estimate how much the embeddings are clustered in the embedding space compared to random distribution on a sphere. The downside of this metric is the requirement of pairwise computations, which is expensive for large number of points. We now proceed to study the proposed metrics on real-world data.

4. Experiments

In contrast to previous work (Agrawal et al., 2022; Garido et al., 2022), we shift our attention from self-supervised learning to novel, more generally applicable settings. We experimentally study proposed metrics on two novel use-cases: (i) supervised representation learning with deep neural networks and (ii) unsupervised graph embeddings. Supervised representation learning allows us to gain insights into performance of semi-supervised learning systems. Graph embedding, on the other hand, has very different architecture—shallow single-layer network—and optimization.

Section 4.1.2 further provides a novel study on computational stability of different embedding quality evaluation metrics. Stability is important for many practical application, since the most computationally stable metrics can be even computed during training for monitoring purposes.

4.1. Supervised Network Performance Prediction

We used Wightman (2019) repository of supervised PyTorch models, accessed May 2023. (Deng et al., 2009) We ran inference of all available models, as permitted by GPU memory, on the validation set, and a subset of models¹—on the full training set. Inference was performed on a single 16-core machine with NVIDIA RTX 4090 and 64Gb RAM.

4.1.1. DOWNSTREAM QUALITY CORRELATION

Figures 1 and 2 present rank correlation of the different embedding quality metrics to downstream prediction quality on ImageNet, measured for training and validation set embeddings respectively. We do not report SelfCluster metric results on the training set because of its quadratic time complexity. Since RankMe is dependent on the dimensionality of the data, we normalize its values and call the metric RankMe*. This new metric has the range between 0 and 1, and represents relative utilization of the embedding space.

On the training set evaluation, α -ReQ, NESum, pseudo-condition number, and coherence all show significant correlation to the test set performance. Out of these metrics, α -ReQ is the only metric with significant outliers, possibly due to the power law estimation issues (Clauset et al., 2009). High stable rank, NESum, and coherence seem to indicate good test set performance of the model. Note that the models we selected for training set evaluation are pareto-optimal in terms of either parameter size or inference speed. This allowed us to significantly restrict the model set size without affecting representativeness of selected models.

On the validation set performance with expanded model set, the correlation between many metrics and test set performance drops to near-zero. This can be attributed to both

¹Full list available in the Appendix.

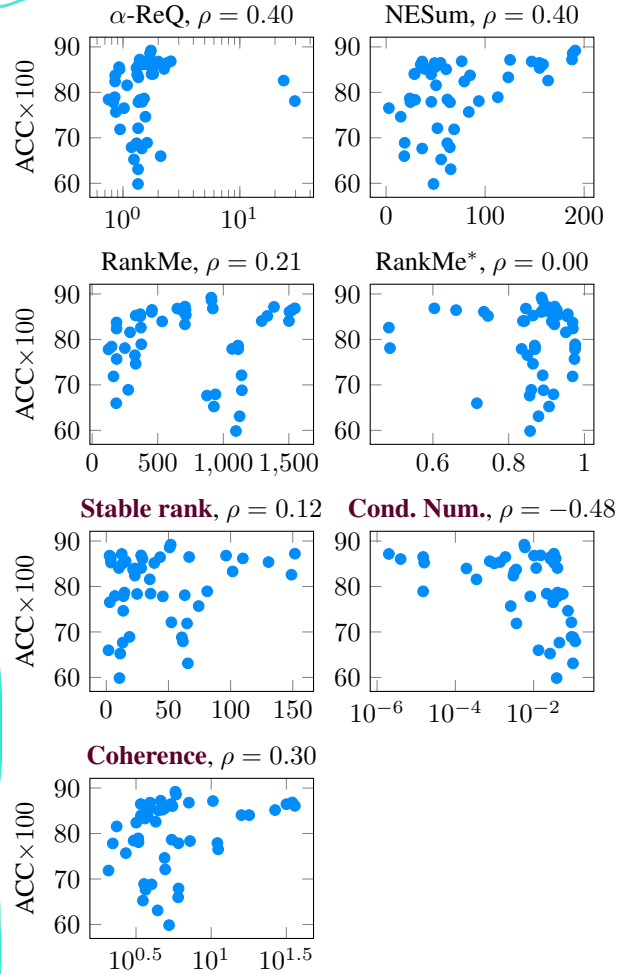


Figure 1. Representation quality metrics on the ImageNet training set for over 30 pre-trained models. Spearman rank correlation ρ to the test set accuracy displayed per metric in the title. Methods introduced in this work are highlighted in colored bold.

expanded model set, which has many under-performing models as well as the general instability of the computation on the smaller example set. We further examine the computational stability considerations in the next section. Only NESum, stable rank and self clustering achieve significant correlation to the test set performance. Across both training and validation sets, NESum demonstrates strong downstream performance correlation while both variants of RankMe are not able to successfully predict supervised task performance.

4.1.2. METRIC STABILITY

It is important to have stable metrics for embedding quality evaluation, especially in low-data regimes. Moreover, if a metric is stable up to very small batch sizes, it can be evaluated during training, greatly enhancing its usability.

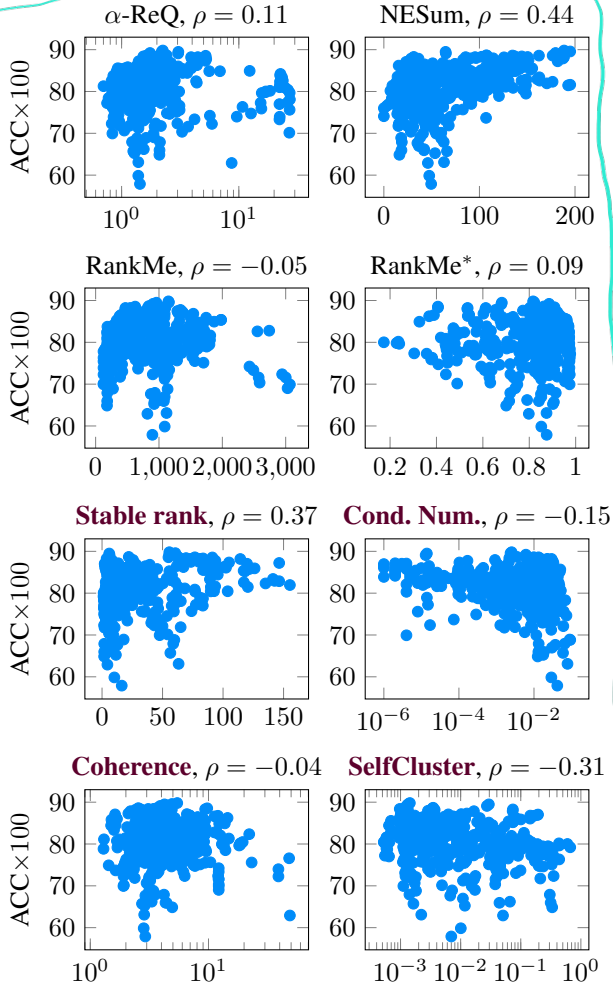


Figure 2. Representation quality metrics on the ImageNet validation set of over 1000 pre-trained models. Spearman rank correlation ρ to the test set accuracy displayed per metric in the title. Methods introduced in this work are highlighted in colored bold.

To do that, we sample embeddings for ImageNet training set with batch sizes from 128 to 65536, log-space (2^7 – 2^{16}) and compare the sampled metric value to the value computed on the whole dataset. The results are presented in Table 1. Numerical rank-based methods are among the most stable, followed by NESum. One advantage of RankMe over its numerical rank estimation counterpart is that it offers a strong lower-bound in terms of the sample size. Coherence appears to be strongly data-dependent and least stable.

4.2. Graph Embedding Quality Prediction

Graph embedding is a common way to solve many tasks arising in the graph mining domain from node classification, link prediction, and community detection. In the graph embedding process, each node in a graph is mapped to a vector in \mathbb{R}^d , and distances in the embedding space should resemble some similarity metric defined between the nodes

Table 1. Batch sizes needed to achieve constant multiplicative approximation factors compared to evaluation on the full ImageNet training set on XX networks. Additionally, we check that each metric lower-bounds the true value. The result can be either ✓yes, ✗no, or ✳0.95-approximately.

| metric | Bounded | Approximation factor | | | |
|---------------|---------|----------------------|------|-------|-------|
| | | 0.5 | 0.7 | 0.9 | 0.95 |
| α -ReQ | ✗ | 512 | 4096 | 32768 | — |
| NESum | ✳ | 1024 | 2048 | 8192 | 32768 |
| RankMe | ✓ | 2048 | 2048 | 8192 | 16384 |
| Stable rank | ✳ | 512 | 2048 | 8192 | 16384 |
| Cond. number | ✗ | 4096 | 4096 | 32768 | 65536 |
| Coherence | ✓ | — | — | — | — |

Table 2. Dataset statistics. We report total number of nodes $|V|$, average node degree \bar{d} , number of labels $|Y|$.

| dataset | $ V $ | \bar{d} | $ Y $ |
|--------------|--------|-----------|-------|
| Cora | 19793 | 3.20 | 7 |
| Citeseer | 3327 | 1.37 | 6 |
| PubMed | 19717 | 2.25 | 3 |
| Amazon PC | 13752 | 17.88 | 10 |
| Amazon Photo | 7650 | 15.57 | 8 |
| MSA-Physics | 34493 | 7.19 | 5 |
| OGB-arXiv | 169343 | 6.84 | 40 |
| CIFAR-10 | 50000 | 99 | 10 |
| MNIST | 60000 | 99 | 10 |

in the original graph (Tsitsulin et al., 2018). For an in-depth review of modern graph embedding approaches, readers are referred to Chami et al. (2022) survey.

For our experiments, we study representations of the DeepWalk (Perozzi et al., 2014) model as it is a de-facto standard in the field of unsupervised embedding of graphs with no features. We use 10 different graph datasets that include both natural and constructed graphs. We report the dataset statistics in Table 2 and provide a brief description below:

- Cora, Citeseer, and Pubmed (Sen et al., 2008) are citation networks; nodes represent papers connected by citation edges; features are bag-of-word abstracts, and labels represent paper topics. We use a re-processed version of Cora from (Shchur et al., 2018) due to errors in the processing of the original dataset.
- Amazon {PC, Photo} (Shchur et al., 2018) are two subsets of the Amazon co-purchase graph for the computers and photo sections of the website, where nodes represent goods with edges between ones frequently purchased together; node features are bag-of-word reviews, and class labels are product category.
- OGB-ArXiv (Hu et al., 2020) is a paper co-citation dataset based on arXiv papers indexed by the Microsoft Academic graph. Nodes are papers; edges are citations, and class labels indicate the main category of the paper.

Table 3. Average Spearman rank correlation on two dataset corruption types: naïve (N) and component-preserving (C). We highlight datasets where there is a consistent correlation pattern, meaning the same sign and approximately the same magnitude of correlation. Methods proposed in this work exhibit stronger and more consistent correlation patterns across all datasets.

| metric | Cora | | Citeseer | | Pubmed | | Amazon PC | | Amazon Photo | |
|---------------|-------|-------|----------|-------|--------|-------|-----------|-------|--------------|-------|
| | N | C | N | C | N | C | N | C | N | C |
| α -ReQ | -1.00 | -1.00 | -1.00 | -1.00 | -1.00 | 0.43 | 0.01 | 0.98 | 0.01 | 0.97 |
| NESum | 1.00 | 0.03 | 1.00 | 0.10 | 0.94 | -0.66 | 0.09 | -1.00 | -0.15 | -1.00 |
| RankMe | 1.00 | 1.00 | 1.00 | 1.00 | 1.00 | -0.37 | -0.05 | -0.99 | -0.43 | -0.99 |
| Stable rank | 1.00 | 0.66 | 1.00 | 0.30 | 1.00 | 0.66 | 0.31 | -1.00 | 0.09 | -1.00 |
| Cond. number | 1.00 | 0.83 | 1.00 | 1.00 | 1.00 | 0.26 | 0.20 | -0.99 | 0.10 | -1.00 |
| SelfCluster | -1.00 | -1.00 | -1.00 | -0.60 | 1.00 | 1.00 | 1.00 | 0.99 | 1.00 | 1.00 |
| Coherence | 1.00 | 1.00 | 0.90 | 1.00 | 0.94 | 1.00 | 0.99 | 0.98 | 0.99 | 0.98 |

| metric | MSA-Physics | | OGB-arXiv | | MNIST | | CIFAR-10 | |
|---------------|-------------|-------|-----------|-------|-------|-------|----------|-------|
| | N | C | N | C | N | C | N | C |
| α -ReQ | -0.70 | 0.94 | -0.81 | 1.00 | -1.00 | 0.98 | 0.96 | 0.99 |
| NESum | 0.51 | -0.98 | 0.84 | -1.00 | 0.99 | -0.92 | -0.84 | -0.99 |
| RankMe | 0.59 | -0.92 | 0.85 | -1.00 | 1.00 | -0.96 | -0.94 | -1.00 |
| Stable rank | 0.52 | -0.97 | 0.99 | -0.99 | 1.00 | -0.78 | -0.85 | -0.99 |
| Cond. number | 0.52 | -0.97 | 0.92 | -1.00 | 1.00 | -0.96 | -0.95 | -0.99 |
| SelfCluster | 0.96 | 0.98 | 1.00 | 1.00 | 1.00 | 1.00 | 1.00 | 0.99 |
| Coherence | 0.97 | 0.99 | 0.90 | 1.00 | 0.89 | 1.00 | 0.98 | 0.99 |

- CIFAR and MNIST (Krizhevsky et al., 2009; LeCun et al., 1998) are ε -nearest neighbor graphs with ε such that the average node degree is 100.

Instead of changing the parameters of the model, we controllably change the quality of data itself. We sparsify each graph in two different ways:

- **Naïve sparsification:** we randomly pick $n\bar{d}$ edges from the original edge set. This method may produce disconnected components, which are known to be difficult to embed correctly.
- **Component-preserving sparsification:** we first ensure the resulting graph is connected by sampling a random spanning tree. Then, we sample $n(\bar{d} - 1)$ edges randomly and output the combined graph.

It is easy to see both versions create a controllably worse version of the data. As such, one could expect that representation quality degrades with the sparsity of the input graph, perhaps faster for the naïve algorithm, since it does not preserve the component information. As we will observe later, surprisingly, this is very much not the case for many embedding quality metrics we study.

We sparsify to a fixed number of edges corresponding to a target average node degree from the range $[1.1, 10]$. Some graphs in our studies have an average node degree < 10 naturally (cf. Table 2), in this case, we stop at that number. We embed each graph 10 times, run a downstream node classification 100 times, and average the result. We report Spearman rank correlation coefficient ρ (Spearman, 1904) between the classification accuracy and each quality metric.

Table 4. Average Spearman rank correlation on two dataset corruption types: naïve and component-preserving. We highlight rows where there is a consistent correlation pattern. Two methods introduced in this work strongly and consistently correlate with the downstream classification performance.

| metric | Naïve | Connected |
|---------------|-------|-----------|
| α -ReQ | -0.50 | 0.48 |
| NESum | 0.49 | -0.71 |
| RankMe | 0.45 | -0.47 |
| Stable rank | 0.56 | -0.46 |
| Cond. number | 0.53 | -0.43 |
| SelfCluster | 0.55 | 0.60 |
| Coherence | 0.95 | 0.99 |

First, we report aggregated results across all datasets in Table 4. Surprisingly, most metrics completely revert the correlation sign between two sparsification strategies. Only SelfCluster and Coherence are aligned with the downstream evaluation, and between them, Coherence displays a near-perfect correlation with the downstream task performance.

Table 3 provides a more nuanced per-dataset view. We can observe that while some metrics have strong and consistent correlation patterns on some datasets, the trend can be completely reversed on others. This calls for more comprehensive evaluations on multiple datasets and machine learning tasks for embedding quality evaluation metrics. Overall, only coherence provides strong signal in a single direction across all the datasets and perturbation methods.

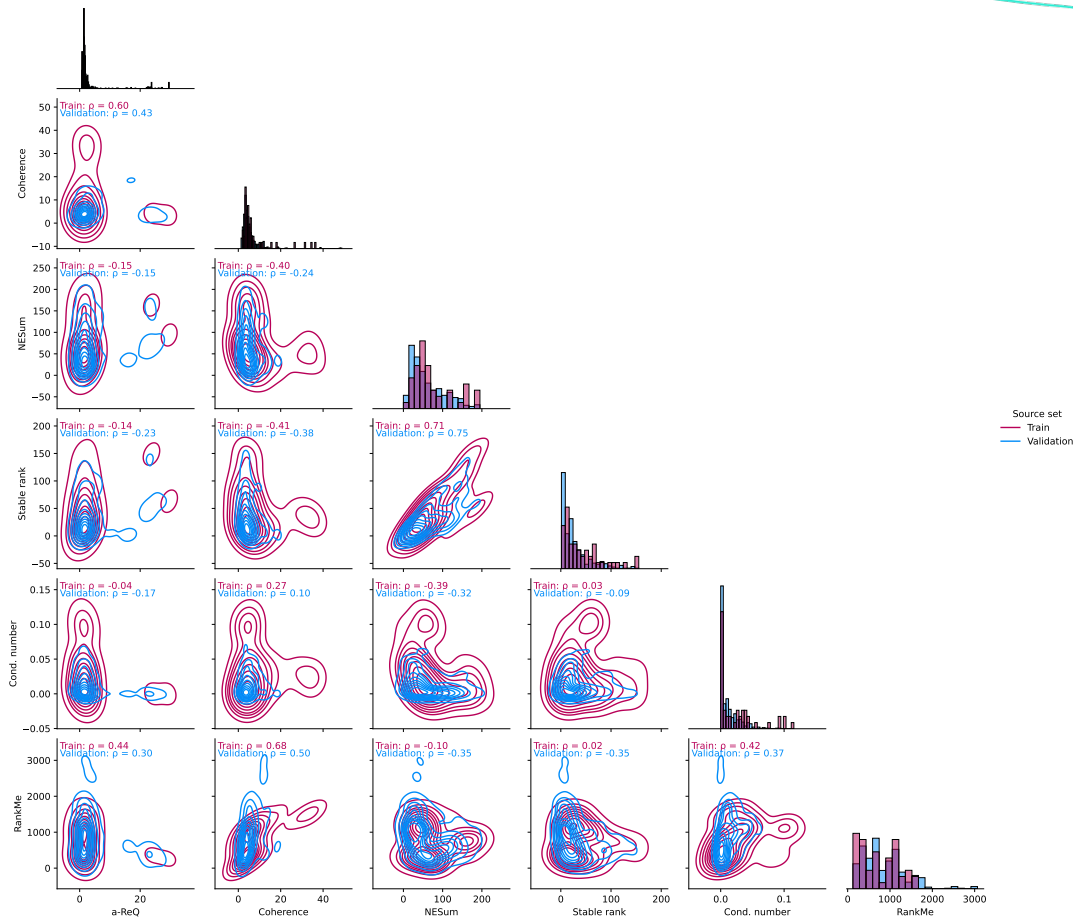


Figure 3. Pairwise density plots of ImageNet representations, as measured on training and validation sets. NESum is well-correlated to Stable rank. Coherence is moderately correlated to α -ReQ and RankMe.

4.3. Metric Similarity

Since there are no clear winners in the experiments, it is important to use multiple metrics in real-world applications. Figure 3 presents pairwise correlations and kernel densities of different metrics on the training and validation sets of ImageNet. Overall, there are two clusters of the metrics: NESum and Stable rank as one and Coherence, α -ReQ, RankMe and condition number in another.

5. Conclusions

Is it possible to estimate embedding quality based on its statistical properties? This paper demonstrates it is possible in two scenarios outside of the known one of self-supervised learning. We introduced four new metrics based on ideas from numerical linear algebra, analysis of linear regression and high-dimensional probability.

We conducted a large-scale study on two novel domains for unsupervised embedding quality evaluation: prediction of supervised test set performance and predicting performance of much simpler single-layer graph embedding methods. In case of supervised models, there seem to be no one-size-fits-all dominant solution, however, we identify numerically stable metrics that have strong correlation with downstream task performance. In the shallow model case, metrics introduced in this work show favorable downstream performance correlation consistently across 9 different datasets.

References

Agrawal, K. K., Mondal, A. K., Ghosh, A., and Richards, B. α -ReQ: Assessing representation quality in self-supervised learning by measuring eigenspectrum decay. *NeurIPS*, 2022. Cited on pages 2 and 4.

- Assran, M., Balestrieri, R., Duval, Q., Bordes, F., Misra, I., Bojanowski, P., Vincent, P., Rabbat, M., and Ballas, N. The hidden uniform cluster prior in self-supervised learning. In *ICLR*, 2023. Cited on page 3.
- Bartlett, P. L., Long, P. M., Lugosi, G., and Tsigler, A. Benign overfitting in linear regression. *PNAS*, 2020. Cited on page 2.
- Belsley, D. A., Kuh, E., and Welsch, R. E. *Regression diagnostics: Identifying influential data and sources of collinearity*. John Wiley & Sons, 2005. Cited on page 3.
- Ben-Israel, A. On error bounds for generalized inverses. *SIAM Journal on Numerical Analysis*, 1966. Cited on page 3.
- Chami, I., Abu-El-Haija, S., Perozzi, B., Ré, C., and Murphy, K. Machine learning on graphs: A model and comprehensive taxonomy. *JMLR*, 2022. Cited on page 5.
- Chen, T., Kornblith, S., Norouzi, M., and Hinton, G. A simple framework for contrastive learning of visual representations. In *ICML*, 2020. Cited on page 1.
- Clauset, A., Shalizi, C. R., and Newman, M. E. Power-law distributions in empirical data. *SIAM review*, 2009. Cited on pages 2 and 4.
- Deng, J., Dong, W., Socher, R., Li, L.-J., Li, K., and Fei-Fei, L. Imagenet: A large-scale hierarchical image database. In *CVPR*, 2009. Cited on page 4.
- Garrido, Q., Balestrieri, R., Najman, L., and Lecun, Y. Rankme: Assessing the downstream performance of pretrained self-supervised representations by their rank. *arXiv preprint arXiv:2210.02885*, 2022. Cited on pages 2 and 4.
- He, B. and Ozay, M. Exploring the gap between collapsed & whitened features in self-supervised learning. In *ICML*, 2022. Cited on page 2.
- Hu, W., Fey, M., Zitnik, M., Dong, Y., Ren, H., Liu, B., Catasta, M., and Leskovec, J. Open graph benchmark: Datasets for machine learning on graphs. *arXiv preprint arXiv:2005.00687*, 2020. Cited on page 5.
- Hua, T., Wang, W., Xue, Z., Ren, S., Wang, Y., and Zhao, H. On feature decorrelation in self-supervised learning. In *CVPR*, 2021. Cited on page 1.
- Krizhevsky, A., Hinton, G., et al. Learning multiple layers of features from tiny images. 2009. Cited on page 6.
- LeCun, Y., Cortes, C., and Burges, C. J. C. The MNIST database of handwritten digits. <http://yann.lecun.com/exdb/mnist/>, 1998. Cited on page 6.
- Mohri, M. and Talwalkar, A. Can matrix coherence be efficiently and accurately estimated? In *AISTATS*, 2011. Cited on pages 2 and 3.
- Perozzi, B., Al-Rfou, R., and Skiena, S. Deepwalk: Online learning of social representations. In *KDD*, 2014. Cited on pages 1 and 5.
- Roy, O. and Vetterli, M. The effective rank: A measure of effective dimensionality. In *European signal processing conference*. IEEE, 2007. Cited on page 2.
- Rudelson, M. and Vershynin, R. Sampling from large matrices: An approach through geometric functional analysis. *Journal of the ACM*, 2007. Cited on page 3.
- Sen, P., Namata, G., Bilgic, M., Getoor, L., Galligher, B., and Eliassi-Rad, T. Collective classification in network data. *AI magazine*, 2008. Cited on page 5.
- Shchur, O., Mumme, M., Bojchevski, A., and Günnemann, S. Pitfalls of graph neural network evaluation. *arXiv preprint arXiv:1811.05868*, 2018. Cited on page 5.
- Spearman, C. The proof and measurement of association between two things. 1904. Cited on page 6.
- Tsitsulin, A., Mottin, D., Karras, P., and Müller, E. Verse: Versatile graph embeddings from similarity measures. In *WWW*, 2018. Cited on page 5.
- Vershynin, R. *High-dimensional probability: An introduction with applications in data science*, volume 47. Cambridge university press, 2018. Cited on page 3.
- Wightman, R. Pytorch image models. <https://github.com/rwightman/pytorch-image-models>, 2019. Cited on page 4.
- Zbontar, J., Jing, L., Misra, I., LeCun, Y., and Deny, S. Barlow twins: Self-supervised learning via redundancy reduction. In *ICML*, 2021. Cited on page 2.

A. Appendix.

Here we present the list of models we used for experimenting on the training and validation sets of ImageNet.

Training set models

beitv2_base_patch16_224.in1k_ft_in22k_in1k
coat_tiny
convnext_base.fb_in22k_ft_in1k_384
convnext_femto_ols.d1_in1k
dla46x_c
edgenext_base
edgenext_small
edgenext_x_small
edgenext_xx_small
eva_giant_patch14_560.m30m_ft_in22k_in1k
eva_large_patch14_196.in22k_ft_in22k_in1k
eva_large_patch14_336.in22k_ft_in22k_in1k
lcnet_050.ra2_in1k
lcnet_075.ra2_in1k
lcnet_100.ra2_in1k
levit_128s
maxvit_base_tf_512.in21k_ft_in1k
maxvit_large_tf_512.in21k_ft_in1k
mobilenetv3_large_100.mii1_in21k_ft_in1k
mobilenetv3_small_075.lamb_in1k
mobilenetv3_small_100.lamb_in1k
mobilevit_xs
mobilevit_xxs
mobilevitv2_100
mobilevitv2_150_384_in22ft1k
regnetz_d8
rexnet_100
swin_large_patch4_window12_384
tf_efficientnet_b0.ns_jft_in1k
tf_efficientnet_b3.ns_jft_in1k
tf_efficientnet_b4.ns_jft_in1k
tf_efficientnet_b5.ns_jft_in1k
tf_efficientnet_b6.ns_jft_in1k
tf_efficientnet_b7.ns_jft_in1k
tf_efficientnetv2_b0.in1k
tf_mobilenetv3_small_100.in1k
tinynet_e.in1k
vit_base_patch16_clip_224.laion2b_ft_in12k_in1k
vit_base_patch16_clip_384.laion2b_ft_in12k_in1k
vit_base_patch32_clip_224.laion2b_ft_in12k_in1k
vit_base_patch32_clip_384.laion2b_ft_in12k_in1k
volo_d1_384
volo_d2_384
volo_d3_448
volo_d4_448
xcit_nano_12_p8_384_dist
xcit_small_12_p8_384_dist
xcit_small_24_p8_384_dist
xcit_tiny_12_p8_384_dist
xcit_tiny_24_p8_384_dist

Validation set models

| | |
|--|--|
| adv_inception_v3 | bat_resnext26ts.ch_in1k |
| beit_base_patch16_224.in22k_ft_in22k | beit_base_patch16_224.in22k_ft_in22k_in1k |
| beit_base_patch16_384.in22k_ft_in22k_in1k | beit_large_patch16_224.in22k_ft_in22k |
| beit_large_patch16_224.in22k_ft_in22k_in1k | beit_large_patch16_384.in22k_ft_in22k_in1k |
| beit_large_patch16_512.in22k_ft_in22k_in1k | beitv2_base_patch16_224.in1k_ft_in22k |
| beitv2_base_patch16_224.in1k_ft_in22k_in1k | beitv2_large_patch16_224.in1k_ft_in22k |
| beitv2_large_patch16_224.in1k_ft_in22k_in1k | botnet26t_256 |
| cait_m36_384 | cait_m48_448 |
| cait_s24_224 | cait_s24_384 |
| cait_s36_384 | cait_xs24_384 |
| cait_xxs24_224 | cait_xxs24_384 |
| cait_xxs36_224 | cait_xxs36_384 |
| coat_lite_mini | coat_lite_small |
| coat_lite_tiny | coat_mini |
| coat_tiny | coatnet_0_rw_224.sw_in1k |
| coatnet_1_rw_224.sw_in1k | coatnet_2_rw_224.sw_in12k |
| coatnet_2_rw_224.sw_in12k_ft_in1k | coatnet_3_rw_224.sw_in12k |
| coatnet_bn_0_rw_224.sw_in1k | coatnet_nano_rw_224.sw_in1k |
| coatnet_rmlp_1_rw2_224.sw_in12k | coatnet_rmlp_1_rw2_224.sw_in12k_ft_in1k |
| coatnet_rmlp_1_rw_224.sw_in1k | coatnet_rmlp_2_rw_224.sw_in12k |
| coatnet_rmlp_2_rw_224.sw_in12k_ft_in1k | coatnet_rmlp_2_rw_224.sw_in1k |
| coatnet_rmlp_2_rw_384.sw_in12k_ft_in1k | coatnet_rmlp_nano_rw_224.sw_in1k |
| coatnext_nano_rw_224.sw_in1k | convit_base |
| convit_small | convit_tiny |
| convmixer_1024_20_ks9_p14 | convmixer_1536_20 |
| convmixer_768_32 | convnext_atto.d2_in1k |
| convnext_atto_ols.a2_in1k | convnext_base.clip_laion2b |
| convnext_base.clip_laion2b_augreg | convnext_base.clip_laion2b_augreg_ft_in12k |
| convnext_base.clip_laion2b_augreg_ft_in12k_in1k | convnext_base.clip_laion2b_augreg_ft_in12k_in1k_384 |
| convnext_base.clip_laion2b_augreg_ft_in1k | convnext_base.clip_laiona |
| convnext_base.clip_laiona_320 | convnext_base.clip_laiona_augreg_320 |
| convnext_base.clip_laiona_augreg_ft_in1k_384 | convnext_base.fb_in1k |
| convnext_base.fb_in22k | convnext_base.fb_in22k_ft_in1k |
| convnext_base.fb_in22k_ft_in1k_384 | convnext_femto.d1_in1k |
| convnext_femto_ols.d1_in1k | convnext_large.fb_in1k |
| convnext_large.fb_in22k | convnext_large.fb_in22k_ft_in1k |
| convnext_large.fb_in22k_ft_in1k_384 | convnext_large_mlp.clip_laion2b_augreg |
| convnext_large_mlp.clip_laion2b_augreg_ft_in12k_384 | convnext_large_mlp.clip_laion2b_augreg_ft_in1k |
| convnext_large_mlp.clip_laion2b_augreg_ft_in1k_384 | convnext_large_mlp.clip_laion2b_ft_320 |
| convnext_large_mlp.clip_laion2b_ft_soup_320 | convnext_large_mlp.clip_laion2b_soup_ft_in12k_320 |
| convnext_large_mlp.clip_laion2b_soup_ft_in12k_384 | convnext_large_mlp.clip_laion2b_soup_ft_in12k_in1k_320 |
| convnext_large_mlp.clip_laion2b_soup_ft_in12k_in1k_384 | convnext_nano.dlh_in1k |
| convnext_nano.in12k | convnext_nano.in12k_ft_in1k |
| convnext_nano_ols.dlh_in1k | convnext_pico.dl_in1k |
| convnext_pico_ols.dl_in1k | convnext_small.fb_in1k |
| convnext_small.fb_in22k | convnext_small.fb_in22k_ft_in1k |
| convnext_small.fb_in22k_ft_in1k_384 | convnext_small.in12k |
| convnext_small.in12k_ft_in1k | convnext_small.in12k_ft_in1k_384 |
| convnext_tiny.fb_in1k | convnext_tiny.fb_in22k |
| convnext_tiny.fb_in22k_ft_in1k | convnext_tiny.fb_in22k_ft_in1k_384 |

Unsupervised Embedding Quality Evaluation

| | |
|--|---|
| convnext_tiny.in12k | convnext_tiny.in12k_ft_in1k |
| convnext_tiny.in12k_ft_in1k_384 | convnext_tiny_hnf.a2h_in1k |
| convnext_xlarge.fb_in22k | convnext_xlarge.fb_in22k_ft_in1k |
| convnext_xlarge.fb_in22k_ft_in1k_384 | convnext_xlarge.clip_laion2b_rewind |
| convnext_xlarge.clip_laion2b_soup | convnext_xlarge.clip_laion2b_soup_ft_in1k |
| convnextv2_atto.fcmae | convnextv2_atto.fcmae_ft_in1k |
| convnextv2_base.fcmae | convnextv2_base.fcmae_ft_in1k |
| convnextv2_base.fcmae_ft_in22k_in1k | convnextv2_base.fcmae_ft_in22k_in1k_384 |
| convnextv2_femto.fcmae | convnextv2_femto.fcmae_ft_in1k |
| convnextv2_huge.fcmae | convnextv2_huge.fcmae_ft_in1k |
| convnextv2_huge.fcmae_ft_in22k_in1k_384 | convnextv2_huge.fcmae_ft_in22k_in1k_512 |
| convnextv2_large.fcmae | convnextv2_large.fcmae_ft_in1k |
| convnextv2_large.fcmae_ft_in22k_in1k | convnextv2_large.fcmae_ft_in22k_in1k_384 |
| convnextv2_nano.fcmae | convnextv2_nano.fcmae_ft_in1k |
| convnextv2_nano.fcmae_ft_in22k_in1k | convnextv2_nano.fcmae_ft_in22k_in1k_384 |
| convnextv2_pico.fcmae | convnextv2_pico.fcmae_ft_in1k |
| convnextv2_tiny.fcmae | convnextv2_tiny.fcmae_ft_in1k |
| convnextv2_tiny.fcmae_ft_in22k_in1k | convnextv2_tiny.fcmae_ft_in22k_in1k_384 |
| crossvit_15_240 | crossvit_15_dagger_240 |
| crossvit_15_dagger_408 | crossvit_18_240 |
| crossvit_18_dagger_240 | crossvit_18_dagger_408 |
| crossvit_9_240 | crossvit_9_dagger_240 |
| crossvit_base_240 | crossvit_small_240 |
| crossvit_tiny_240 | cs3darknet_focus_l |
| cs3darknet_focus_m | cs3darknet_l |
| cs3darknet_m | cs3darknet_x |
| cs3edgenet_x | cs3se_edgenet_x |
| cs3sedarknet_l | cs3sedarknet_x |
| cspdarknet53 | cspresnet50 |
| cspresnext50 | darknet53 |
| darknetaa53 | davit_base.msft_in1k |
| davit_small.msft_in1k | davit_tiny.msft_in1k |
| deit3_base_patch16_224.fb_in1k | deit3_base_patch16_224.fb_in22k_ft_in1k |
| deit3_base_patch16_384.fb_in1k | deit3_base_patch16_384.fb_in22k_ft_in1k |
| deit3_huge_patch14_224.fb_in1k | deit3_huge_patch14_224.fb_in22k_ft_in1k |
| deit3_large_patch16_224.fb_in1k | deit3_large_patch16_224.fb_in22k_ft_in1k |
| deit3_large_patch16_384.fb_in1k | deit3_large_patch16_384.fb_in22k_ft_in1k |
| deit3_medium_patch16_224.fb_in1k | deit3_medium_patch16_224.fb_in22k_ft_in1k |
| deit3_small_patch16_224.fb_in1k | deit3_small_patch16_224.fb_in22k_ft_in1k |
| deit3_small_patch16_384.fb_in1k | deit3_small_patch16_384.fb_in22k_ft_in1k |
| deit_base_distilled_patch16_224.fb_in1k | deit_base_distilled_patch16_384.fb_in1k |
| deit_base_patch16_224.fb_in1k | deit_base_patch16_384.fb_in1k |
| deit_small_distilled_patch16_224.fb_in1k | deit_small_patch16_224.fb_in1k |
| deit_tiny_distilled_patch16_224.fb_in1k | deit_tiny_patch16_224.fb_in1k |
| densenet121 | densenet161 |
| densenet169 | densenet201 |
| densenetblur121d | dla102 |
| dla102x | dla102x2 |
| dla169 | dla34 |
| dla46_c | dla46x_c |
| dla60 | dla60_res2net |
| dla60_res2next | dla60x |
| dla60x_c | dm_nfnet_f0.dm_in1k |
| dm_nfnet_f1.dm_in1k | dm_nfnet_f2.dm_in1k |

Unsupervised Embedding Quality Evaluation

| | |
|---|--|
| dm_nfnet_f3.dm_in1k | dm_nfnet_f4.dm_in1k |
| dm_nfnet_f5.dm_in1k | dm_nfnet_f6.dm_in1k |
| dpn107 | dpn131 |
| dpn68 | dpn68b |
| dpn92 | dpn98 |
| eca_botnext26ts_256 | eca_halonext26ts |
| eca_nfnet_l0.ra2_in1k | eca_nfnet_l1.ra2_in1k |
| eca_nfnet_l2.ra3_in1k | eca_resnet33ts.ra2_in1k |
| eca_resnext26ts.ch_in1k | ecaresnet101d.miil_in1k |
| ecaresnet101d_pruned.miil_in1k | ecaresnet269d.ra2_in1k |
| ecaresnet26t.ra2_in1k | ecaresnet50d.miil_in1k |
| ecaresnet50d_pruned.miil_in1k | ecaresnet50t.a1_in1k |
| ecaresnet50t.a2_in1k | ecaresnet50t.a3_in1k |
| ecaresnet50t.ra2_in1k | ecaresnetlight.miil_in1k |
| edgenext_base | edgenext_small |
| edgenext_small_rw | edgenext_x_small |
| edgenext_xx_small | efficientformer_l1.snap_dist_in1k |
| efficientformer_l3.snap_dist_in1k | efficientformer_l7.snap_dist_in1k |
| efficientformerv2_l.snap_dist_in1k | efficientformerv2_s0.snap_dist_in1k |
| efficientformerv2_s1.snap_dist_in1k | efficientformerv2_s2.snap_dist_in1k |
| efficientnet_b0.ra_in1k | efficientnet_b1.ft_in1k |
| efficientnet_b1_pruned.in1k | efficientnet_b2.ra_in1k |
| efficientnet_b2_pruned.in1k | efficientnet_b3.ra2_in1k |
| efficientnet_b3_pruned.in1k | efficientnet_b4.ra2_in1k |
| efficientnet_b5.in12k | efficientnet_b5.in12k_ft_in1k |
| efficientnet_el.ra_in1k | efficientnet_el_pruned.in1k |
| efficientnet_em.ra2_in1k | efficientnet_es.ra_in1k |
| efficientnet_es_pruned.in1k | efficientnet_lite0.ra_in1k |
| efficientnetv2_rw_m.agc_in1k | efficientnetv2_rw_s.ra2_in1k |
| efficientnetv2_rw_t.ra2_in1k | ens_adv_inception_resnet_v2 |
| ese_vovnet19b_dw | ese_vovnet39b |
| eva02_base_patch14_224.mim_in22k | eva02_base_patch14_448.mim_in22k_ft_in1k |
| eva02_base_patch14_448.mim_in22k_ft_in22k | eva02_base_patch14_448.mim_in22k_ft_in22k_in1k |
| eva02_large_patch14_224.mim_in22k | eva02_large_patch14_224.mim_m38m |
| eva02_large_patch14_448.mim_in22k_ft_in1k | eva02_large_patch14_448.mim_in22k_ft_in22k |
| eva02_large_patch14_448.mim_in22k_ft_in22k_in1k | eva02_large_patch14_448.mim_m38m_ft_in1k |
| eva02_large_patch14_448.mim_m38m_ft_in22k | eva02_large_patch14_448.mim_m38m_ft_in22k_in1k |
| eva02_small_patch14_224.mim_in22k | eva02_small_patch14_336.mim_in22k_ft_in1k |
| eva02_tiny_patch14_224.mim_in22k | eva02_tiny_patch14_336.mim_in22k_ft_in1k |
| eva_giant_patch14_224.clip_ft_in1k | eva_giant_patch14_336.clip_ft_in1k |
| eva_giant_patch14_336.m30m_ft_in22k_in1k | eva_giant_patch14_560.m30m_ft_in22k_in1k |
| eva_large_patch14_196.in22k_ft_in1k | eva_large_patch14_196.in22k_ft_in22k_in1k |
| eva_large_patch14_336.in22k_ft_in1k | eva_large_patch14_336.in22k_ft_in22k_in1k |
| fbnetc_100.rmisp_in1k | fbnetv3_b.ra2_in1k |
| fbnetv3_d.ra2_in1k | fbnetv3_g.ra2_in1k |
| flexivit_base.1000ep_in21k | flexivit_base.1200ep_in1k |
| flexivit_base.300ep_in1k | flexivit_base.300ep_in21k |
| flexivit_base.600ep_in1k | flexivit_base.patch16_in21k |
| flexivit_base.patch30_in21k | flexivit_large.1200ep_in1k |
| flexivit_large.300ep_in1k | flexivit_large.600ep_in1k |
| flexivit_small.1200ep_in1k | flexivit_small.300ep_in1k |
| flexivit_small.600ep_in1k | focalnet_base_lrf.ms_in1k |
| focalnet_base_srf.ms_in1k | focalnet_huge_fl3.ms_in22k |
| focalnet_huge_fl4.ms_in22k | focalnet_large_fl3.ms_in22k |

Unsupervised Embedding Quality Evaluation

| | |
|--|--|
| focalnet_large_fl4.ms_in22k | focalnet_small_lrf.ms_in1k |
| focalnet_small_srf.ms_in1k | focalnet_tiny_lrf.ms_in1k |
| focalnet_tiny_srf.ms_in1k | focalnet_xlarge_fl3.ms_in22k |
| focalnet_xlarge_fl4.ms_in22k | gc_efficientnetv2_rw_t.agc_in1k |
| gcrsnet33ts.ra2_in1k | gcrsnet50t.ra2_in1k |
| gcrsnext26ts.ch_in1k | gcrsnext50ts.ch_in1k |
| gcvit_base | gcvit_small |
| gcvit_tiny | gcvit_xtiny |
| gcvit_xxtiny | gernet_l.idstcv_in1k |
| gernet_m.idstcv_in1k | gernet_s.idstcv_in1k |
| ghostnet_100 | gluon_inception_v3 |
| gluon_xception65 | gmixer_24_224.ra3_in1k |
| gmlp_s16_224.ra3_in1k | halo2botnet50ts_256 |
| halonet26t | halonet50ts |
| haloregnetz_b | hardcorenas_a |
| hardcorenas_b | hardcorenas_c |
| hardcorenas_d | hardcorenas_e |
| hardcorenas_f | hrnet_w18 |
| hrnet_w18_small | hrnet_w18_small_v2 |
| hrnet_w30 | hrnet_w32 |
| hrnet_w40 | hrnet_w44 |
| hrnet_w48 | hrnet_w64 |
| inception_resnet_v2 | inception_v3 |
| inception_v4 | jx_nest_base |
| jx_nest_small | jx_nest_tiny |
| lambda_resnet26rpt_256 | lambda_resnet26t |
| lambda_resnet50ts | lamhalobotnet50ts_256 |
| lcnet_050.ra2_in1k | lcnet_075.ra2_in1k |
| lcnet_100.ra2_in1k | legacy_senet154 |
| legacy_seresnet101 | legacy_seresnet152 |
| legacy_seresnet18 | legacy_seresnet34 |
| legacy_seresnet50 | legacy_seresnext101_32x4d |
| legacy_seresnext26_32x4d | legacy_seresnext50_32x4d |
| levit_128.fb_dist_in1k | levit_128s.fb_dist_in1k |
| levit_128s | levit_192.fb_dist_in1k |
| levit_256.fb_dist_in1k | levit_384.fb_dist_in1k |
| levit_conv_128.fb_dist_in1k | levit_conv_128s.fb_dist_in1k |
| levit_conv_192.fb_dist_in1k | levit_conv_256.fb_dist_in1k |
| levit_conv_384.fb_dist_in1k | maxvit_base_tf_224.in1k |
| maxvit_base_tf_384.in1k | maxvit_base_tf_384.in21k_ft_in1k |
| maxvit_base_tf_512.in1k | maxvit_base_tf_512.in21k_ft_in1k |
| maxvit_large_tf_224.in1k | maxvit_large_tf_384.in1k |
| maxvit_large_tf_384.in21k_ft_in1k | maxvit_large_tf_512.in1k |
| maxvit_large_tf_512.in21k_ft_in1k | maxvit_nano_rw_256.sw_in1k |
| maxvit_rmlp_base_rw_224.sw_in12k | maxvit_rmlp_base_rw_224.sw_in12k_ft_in1k |
| maxvit_rmlp_base_rw_384.sw_in12k_ft_in1k | maxvit_rmlp_nano_rw_256.sw_in1k |
| maxvit_rmlp_pico_rw_256.sw_in1k | maxvit_rmlp_small_rw_224.sw_in1k |
| maxvit_rmlp_tiny_rw_256.sw_in1k | maxvit_small_tf_224.in1k |
| maxvit_small_tf_384.in1k | maxvit_small_tf_512.in1k |
| maxvit_tiny_rw_224.sw_in1k | maxvit_tiny_tf_224.in1k |
| maxvit_tiny_tf_384.in1k | maxvit_tiny_tf_512.in1k |
| maxvit_xlarge_tf_384.in21k_ft_in1k | maxvit_xlarge_tf_512.in21k_ft_in1k |
| maxxvit_rmlp_nano_rw_256.sw_in1k | maxxvit_rmlp_small_rw_256.sw_in1k |
| maxxvitv2_nano_rw_256.sw_in1k | maxxvitv2_rmlp_base_rw_224.sw_in12k |

Unsupervised Embedding Quality Evaluation

| | |
|---|---|
| maxxvitv2_rmlp_base_rw_224.sw_in12k_ft_in1k | maxxvitv2_rmlp_base_rw_384.sw_in12k_ft_in1k |
| mixer_b16_224.goog_in21k | mixer_b16_224.goog_in21k_ft_in1k |
| mixer_b16_224.miil_in21k | mixer_b16_224.miil_in21k_ft_in1k |
| mixer_l16_224.goog_in21k | mixer_l16_224.goog_in21k_ft_in1k |
| mixnet_l.ft_in1k | mixnet_m.ft_in1k |
| mixnet_s.ft_in1k | mixnet_xl.ra_in1k |
| mnasnet_100.rmisp_in1k | mnasnet_small.lamb_in1k |
| mobilenetv2_050.lamb_in1k | mobilenetv2_100.ra_in1k |
| mobilenetv2_110d.ra_in1k | mobilenetv2_120d.ra_in1k |
| mobilenetv2_140.ra_in1k | mobilenetv3_large_100.miil_in21k |
| mobilenetv3_large_100.miil_in21k_ft_in1k | mobilenetv3_large_100.ra_in1k |
| mobilenetv3_rw.rmisp_in1k | mobilenetv3_small_050.lamb_in1k |
| mobilenetv3_small_075.lamb_in1k | mobilenetv3_small_100.lamb_in1k |
| mobilevit_s | mobilevit_xs |
| mobilevit_xxs | mobilevitv2_050 |
| mobilevitv2_075 | mobilevitv2_100 |
| mobilevitv2_125 | mobilevitv2_150 |
| mobilevitv2_150_384_in22ft1k | mobilevitv2_150_in22ft1k |
| mobilevitv2_175 | mobilevitv2_175_384_in22ft1k |
| mobilevitv2_175_in22ft1k | mobilevitv2_200 |
| mobilevitv2_200_384_in22ft1k | mobilevitv2_200_in22ft1k |
| mvitv2_base | mvitv2_large |
| mvitv2_small | mvitv2_tiny |
| nasnetalarge | nf_regnet_b1.ra2_in1k |
| nf_resnet50.ra2_in1k | nfnet_l0.ra2_in1k |
| pit_b_224 | pit_b_distilled_224 |
| pit_s_224 | pit_s_distilled_224 |
| pit_ti_224 | pit_ti_distilled_224 |
| pit_xs_224 | pit_xs_distilled_224 |
| pnasnet5large | poolformer_m36 |
| poolformer_m48 | poolformer_s12 |
| poolformer_s24 | poolformer_s36 |
| pvt_v2_b0 | pvt_v2_b1 |
| pvt_v2_b2 | pvt_v2_b2_li |
| pvt_v2_b3 | pvt_v2_b4 |
| pvt_v2_b5 | regnetv_040.ra3_in1k |
| regnetv_064.ra3_in1k | regnetx_002.pycls_in1k |
| regnetx_004.pycls_in1k | regnetx_004_tv.tv2_in1k |
| regnetx_006.pycls_in1k | regnetx_008.pycls_in1k |
| regnetx_008.tv2_in1k | regnetx_016.pycls_in1k |
| regnetx_016.tv2_in1k | regnetx_032.pycls_in1k |
| regnetx_032.tv2_in1k | regnetx_040.pycls_in1k |
| regnetx_064.pycls_in1k | regnetx_080.pycls_in1k |
| regnetx_080.tv2_in1k | regnetx_120.pycls_in1k |
| regnetx_160.pycls_in1k | regnetx_160.tv2_in1k |
| regnetx_320.pycls_in1k | regnetx_320.tv2_in1k |
| regnety_002.pycls_in1k | regnety_004.pycls_in1k |
| regnety_004.tv2_in1k | regnety_006.pycls_in1k |
| regnety_008.pycls_in1k | regnety_008_tv.tv2_in1k |
| regnety_016.pycls_in1k | regnety_016.tv2_in1k |
| regnety_032.pycls_in1k | regnety_032.ra_in1k |
| regnety_032.tv2_in1k | regnety_040.pycls_in1k |
| regnety_040.ra3_in1k | regnety_064.pycls_in1k |
| regnety_064.ra3_in1k | regnety_080.pycls_in1k |

Unsupervised Embedding Quality Evaluation

| | |
|---------------------------------|-------------------------------------|
| regnety_080.ra3_in1k | regnety_080.tv.tv2_in1k |
| regnety_120.pycls_in1k | regnety_120.sw_in12k |
| regnety_120.sw_in12k_ft_in1k | regnety_1280.seer |
| regnety_1280.seer_ft_in1k | regnety_1280.swag_ft_in1k |
| regnety_1280.swag_lc_in1k | regnety_160.deit_in1k |
| regnety_160.lion_in12k_ft_in1k | regnety_160.pycls_in1k |
| regnety_160.sw_in12k | regnety_160.sw_in12k_ft_in1k |
| regnety_160.swag_ft_in1k | regnety_160.swag_lc_in1k |
| regnety_160.tv2_in1k | regnety_2560.seer_ft_in1k |
| regnety_320.pycls_in1k | regnety_320.seer |
| regnety_320.seer_ft_in1k | regnety_320.swag_ft_in1k |
| regnety_320.swag_lc_in1k | regnety_320.tv2_in1k |
| regnety_640.seer | regnety_640.seer_ft_in1k |
| regnetz_040.ra3_in1k | regnetz_040_h.ra3_in1k |
| regnetz_b16.ra3_in1k | regnetz_c16.ra3_in1k |
| regnetz_c16_evos.ch_in1k | regnetz_d32.ra3_in1k |
| regnetz_d8 | regnetz_d8.ra3_in1k |
| regnetz_d8_evos.ch_in1k | regnetz_e8.ra3_in1k |
| repvgg_a2.rvgg_in1k | repvgg_b0.rvgg_in1k |
| repvgg_b1.rvgg_in1k | repvgg_b1g4.rvgg_in1k |
| repvgg_b2.rvgg_in1k | repvgg_b2g4.rvgg_in1k |
| repvgg_b3.rvgg_in1k | repvgg_b3g4.rvgg_in1k |
| res2net101_26w_4s | res2net50_14w_8s |
| res2net50_26w_4s | res2net50_26w_6s |
| res2net50_26w_8s | res2net50_48w_2s |
| res2next50 | resmlp_12_224.fb_dino |
| resmlp_12_224.fb_distilled_in1k | resmlp_12_224.fb_in1k |
| resmlp_24_224.fb_dino | resmlp_24_224.fb_distilled_in1k |
| resmlp_24_224.fb_in1k | resmlp_36_224.fb_distilled_in1k |
| resmlp_36_224.fb_in1k | resmlp_big_24_224.fb_distilled_in1k |
| resmlp_big_24_224.fb_in1k | resmlp_big_24_224.fb_in22k_ft_in1k |
| resnest101e | resnest14d |
| resnest200e | resnest269e |
| resnest26d | resnest50d |
| resnest50d_ls4x24d | resnest50d_4s2x40d |
| resnet101.a1_in1k | resnet101.alh_in1k |
| resnet101.a2_in1k | resnet101.a3_in1k |
| resnet101.gluon_in1k | resnet101.tv2_in1k |
| resnet101.tv_in1k | resnet101c.gluon_in1k |
| resnet101d.gluon_in1k | resnet101d.ra2_in1k |
| resnet101s.gluon_in1k | resnet10t.c3_in1k |
| resnet14t.c3_in1k | resnet152.a1_in1k |
| resnet152.alh_in1k | resnet152.a2_in1k |
| resnet152.a3_in1k | resnet152.gluon_in1k |
| resnet152.tv2_in1k | resnet152.tv_in1k |
| resnet152c.gluon_in1k | resnet152d.gluon_in1k |
| resnet152d.ra2_in1k | resnet152s.gluon_in1k |
| resnet18.a1_in1k | resnet18.a2_in1k |
| resnet18.a3_in1k | resnet18.fb_ssl_yfcc100m_ft_in1k |
| resnet18.fb_swsl_ig1b_ft_in1k | resnet18.gluon_in1k |
| resnet18.tv_in1k | resnet18d.ra2_in1k |
| resnet200d.ra2_in1k | resnet26.bt_in1k |
| resnet26d.bt_in1k | resnet26t.ra2_in1k |
| resnet32ts.ra2_in1k | resnet33ts.ra2_in1k |

Unsupervised Embedding Quality Evaluation

| | |
|---|---|
| resnet34.a1_in1k | resnet34.a2_in1k |
| resnet34.a3_in1k | resnet34.bt_in1k |
| resnet34.gluon_in1k | resnet34.tv_in1k |
| resnet34d.ra2_in1k | resnet50.a1_in1k |
| resnet50.a1h_in1k | resnet50.a2_in1k |
| resnet50.a3_in1k | resnet50.am_in1k |
| resnet50.b1k_in1k | resnet50.b2k_in1k |
| resnet50.bt_in1k | resnet50.c1_in1k |
| resnet50.c2_in1k | resnet50.d_in1k |
| resnet50.fb_ssl_yfcc100m_ft_in1k | resnet50.fb_sws1_ig1b_ft_in1k |
| resnet50.gluon_in1k | resnet50.ra_in1k |
| resnet50.ram_in1k | resnet50.tv2_in1k |
| resnet50.tv_in1k | resnet50.gn.a1h_in1k |
| resnet50c.gluon_in1k | resnet50d.a1_in1k |
| resnet50d.a2_in1k | resnet50d.a3_in1k |
| resnet50d.gluon_in1k | resnet50d.ra2_in1k |
| resnet50s.gluon_in1k | resnet51q.ra2_in1k |
| resnet61q.ra2_in1k | resnetaa101d.sw_in12k |
| resnetaa101d.sw_in12k_ft_in1k | resnetaa50.a1h_in1k |
| resnetaa50d.d_in12k | resnetaa50d.sw_in12k |
| resnetaa50d.sw_in12k_ft_in1k | resnetblur50.bt_in1k |
| resnetrs101.tf_in1k | resnetrs152.tf_in1k |
| resnetrs200.tf_in1k | resnetrs270.tf_in1k |
| resnetrs350.tf_in1k | resnetrs420.tf_in1k |
| resnetrs50.tf_in1k | resnetv2_101.a1h_in1k |
| resnetv2_101x1_bit.goog_in21k | resnetv2_101x1_bit.goog_in21k_ft_in1k |
| resnetv2_101x3_bit.goog_in21k | resnetv2_101x3_bit.goog_in21k_ft_in1k |
| resnetv2_152x2_bit.goog_in21k | resnetv2_152x2_bit.goog_in21k_ft_in1k |
| resnetv2_152x2_bit.goog_teacher_in21k_ft_in1k | resnetv2_152x2_bit.goog_teacher_in21k_ft_in1k_384 |
| resnetv2_152x4_bit.goog_in21k | resnetv2_152x4_bit.goog_in21k_ft_in1k |
| resnetv2_50.a1h_in1k | resnetv2_50d_evos.ah_in1k |
| resnetv2_50d_gn.ah_in1k | resnetv2_50x1_bit.goog_distilled_in1k |
| resnetv2_50x1_bit.goog_in21k | resnetv2_50x1_bit.goog_in21k_ft_in1k |
| resnetv2_50x3_bit.goog_in21k | resnetv2_50x3_bit.goog_in21k_ft_in1k |
| resnext101_32x16d.fb_ssl_yfcc100m_ft_in1k | resnext101_32x16d.fb_sws1_ig1b_ft_in1k |
| resnext101_32x16d.fb_wsl_ig1b_ft_in1k | resnext101_32x32d.fb_wsl_ig1b_ft_in1k |
| resnext101_32x4d.fb_ssl_yfcc100m_ft_in1k | resnext101_32x4d.fb_sws1_ig1b_ft_in1k |
| resnext101_32x4d.gluon_in1k | resnext101_32x8d.fb_ssl_yfcc100m_ft_in1k |
| resnext101_32x8d.fb_sws1_ig1b_ft_in1k | resnext101_32x8d.fb_wsl_ig1b_ft_in1k |
| resnext101_32x8d.tv2_in1k | resnext101_32x8d.tv_in1k |
| resnext101_64x4d.c1_in1k | resnext101_64x4d.gluon_in1k |
| resnext101_64x4d.tv_in1k | resnext26ts.ra2_in1k |
| resnext50_32x4d.a1_in1k | resnext50_32x4d.a1h_in1k |
| resnext50_32x4d.a2_in1k | resnext50_32x4d.a3_in1k |
| resnext50_32x4d.fb_ssl_yfcc100m_ft_in1k | resnext50_32x4d.fb_sws1_ig1b_ft_in1k |
| resnext50_32x4d.gluon_in1k | resnext50_32x4d.ra_in1k |
| resnext50_32x4d.tv2_in1k | resnext50_32x4d.tv_in1k |
| resnext50d_32x4d.bt_in1k | rexnet_100.nav_in1k |
| rexnet_100 | rexnet_130.nav_in1k |
| rexnet_150.nav_in1k | rexnet_200.nav_in1k |
| rexnet_300.nav_in1k | rexnetr_200.sw_in12k |
| rexnetr_200.sw_in12k_ft_in1k | rexnetr_300.sw_in12k |
| rexnetr_300.sw_in12k_ft_in1k | sebotnet33ts_256 |
| sehalonet33ts | selecls42b |

Unsupervised Embedding Quality Evaluation

| | |
|---|---|
| selecsls60 | selecsls60b |
| semnasnet_075.rmsp_in1k | semnasnet_100.rmsp_in1k |
| senet154.gluon_in1k | sequencer2d_l |
| sequencer2d_m | sequencer2d_s |
| seresnet152d.ra2_in1k | seresnet33ts.ra2_in1k |
| seresnet50.a1_in1k | seresnet50.a2_in1k |
| seresnet50.a3_in1k | seresnet50.ra2_in1k |
| seresnext101_32x4d.gluon_in1k | seresnext101_32x8d.ah_in1k |
| seresnext101_64x4d.gluon_in1k | seresnext101d_32x8d.ah_in1k |
| seresnext26d_32x4d.bt_in1k | seresnext26t_32x4d.bt_in1k |
| seresnext26ts.ch_in1k | seresnext50_32x4d.gluon_in1k |
| seresnext50_32x4d.racm_in1k | seresnextaa101d_32x8d.ah_in1k |
| seresnextaa101d_32x8d.sw_in12k | seresnextaa101d_32x8d.sw_in12k_ft_in1k |
| seresnextaa101d_32x8d.sw_in12k_ft_in1k_288 | skresnet18 |
| skresnet34 | skresnext50_32x4d |
| spnasnet_100.rmsp_in1k | swin_base_patch4_window12_384.ms_in1k |
| swin_base_patch4_window12_384.ms_in22k | swin_base_patch4_window12_384.ms_in22k_ft_in1k |
| swin_base_patch4_window7_224.ms_in1k | swin_base_patch4_window7_224.ms_in22k |
| swin_base_patch4_window7_224.ms_in22k_ft_in1k | swin_large_patch4_window12_384.ms_in22k |
| swin_large_patch4_window12_384.ms_in22k_ft_in1k | swin_large_patch4_window12_384 |
| swin_large_patch4_window7_224.ms_in22k | swin_large_patch4_window7_224.ms_in22k_ft_in1k |
| swin_s3_base_224.ms_in1k | swin_s3_small_224.ms_in1k |
| swin_s3_tiny_224.ms_in1k | swin_small_patch4_window7_224.ms_in1k |
| swin_small_patch4_window7_224.ms_in22k | swin_small_patch4_window7_224.ms_in22k_ft_in1k |
| swin_tiny_patch4_window7_224.ms_in1k | swin_tiny_patch4_window7_224.ms_in22k |
| swin_tiny_patch4_window7_224.ms_in22k_ft_in1k | swinv2_base_window12_192.ms_in22k |
| swinv2_base_window12to16_192to256.ms_in22k_ft_in1k | swinv2_base_window12to24_192to384.ms_in22k_ft_in1k |
| swinv2_base_window16_256.ms_in1k | swinv2_base_window8_256.ms_in1k |
| swinv2_cr_small_224.sw_in1k | swinv2_cr_small_ns_224.sw_in1k |
| swinv2_cr_tiny_ns_224.sw_in1k | swinv2_large_window12_192.ms_in22k |
| swinv2_large_window12to16_192to256.ms_in22k_ft_in1k | swinv2_large_window12to24_192to384.ms_in22k_ft_in1k |
| swinv2_small_window16_256.ms_in1k | swinv2_small_window8_256.ms_in1k |
| swinv2_tiny_window16_256.ms_in1k | swinv2_tiny_window8_256.ms_in1k |
| tf_efficientnet_b0.aa_in1k | tf_efficientnet_b0.ap_in1k |
| tf_efficientnet_b0.ns_jft_in1k | tf_efficientnet_b1.aa_in1k |
| tf_efficientnet_b1.ap_in1k | tf_efficientnet_b1.ns_jft_in1k |
| tf_efficientnet_b2.aa_in1k | tf_efficientnet_b2.ap_in1k |
| tf_efficientnet_b2.ns_jft_in1k | tf_efficientnet_b3.aa_in1k |
| tf_efficientnet_b3.ap_in1k | tf_efficientnet_b3.ns_jft_in1k |
| tf_efficientnet_b4.aa_in1k | tf_efficientnet_b4.ap_in1k |
| tf_efficientnet_b4.ns_jft_in1k | tf_efficientnet_b5.ap_in1k |
| tf_efficientnet_b5.ns_jft_in1k | tf_efficientnet_b5.ra_in1k |
| tf_efficientnet_b6.aa_in1k | tf_efficientnet_b6.ap_in1k |
| tf_efficientnet_b6.ns_jft_in1k | tf_efficientnet_b7.ap_in1k |
| tf_efficientnet_b7.ns_jft_in1k | tf_efficientnet_b7.ra_in1k |
| tf_efficientnet_b8.ap_in1k | tf_efficientnet_b8.ra_in1k |
| tf_efficientnet_cc_b0_4e.in1k | tf_efficientnet_cc_b0_8e.in1k |
| tf_efficientnet_cc_b1_8e.in1k | tf_efficientnet_el.in1k |
| tf_efficientnet_em.in1k | tf_efficientnet_es.in1k |
| tf_efficientnet_lite0.in1k | tf_efficientnet_lite1.in1k |
| tf_efficientnet_lite2.in1k | tf_efficientnet_lite3.in1k |
| tf_efficientnet_lite4.in1k | tf_efficientnetv2_b0.in1k |
| tf_efficientnetv2_b1.in1k | tf_efficientnetv2_b2.in1k |
| tf_efficientnetv2_b3.in1k | tf_efficientnetv2_b3.in21k |

Unsupervised Embedding Quality Evaluation

tf_efficientnetv2_b3.in21k_ft_in1k
tf_efficientnetv2_l.in21k
tf_efficientnetv2_m.in1k
tf_efficientnetv2_m.in21k_ft_in1k
tf_efficientnetv2_s.in21k
tf_efficientnetv2_xl.in21k
tf_inception_v3
tf_mixnet_m.in1k
tf_mobilenetv3_large_075.in1k
tf_mobilenetv3_large_minimal_100.in1k
tf_mobilenetv3_small_100.in1k
tinynet_a.in1k
tinynet_c.in1k
tinynet_e.in1k
tv_densenet121
twins_pcpvt_large
twins_svt_base
twins_svt_small
vgg11_bn
vgg13_bn
vgg16_bn
vgg19_bn
vit_base_patch16_224.augreg2_in21k_ft_in1k
vit_base_patch16_224.augreg_in21k
vit_base_patch16_224.dino
vit_base_patch16_224.sam
vit_base_patch16_224_miil.in21k_ft_in1k
vit_base_patch16_384.augreg_in21k_ft_in1k
vit_base_patch16_clip_224.laion2b
vit_base_patch16_clip_224.laion2b_ft_in12k_in1k
vit_base_patch16_clip_224.openai
vit_base_patch16_clip_224.openai_ft_in12k_in1k
vit_base_patch16_clip_384.laion2b_ft_in12k_in1k
vit_base_patch16_clip_384.openai_ft_in12k_in1k
vit_base_patch16_rpn_224.in1k
vit_base_patch32_224.augreg_in21k
vit_base_patch32_224.sam
vit_base_patch32_384.augreg_in21k_ft_in1k
vit_base_patch32_clip_224.laion2b_ft_in12k_in1k
vit_base_patch32_clip_224.openai
vit_base_patch32_clip_384.laion2b_ft_in12k_in1k
vit_base_patch32_clip_448.laion2b_ft_in12k_in1k
vit_base_patch8_224.augreg_in21k
vit_base_patch8_224.dino
vit_base_patch8_224.orig_in21k_ft_in1k
vit_gigantic_patch14_clip_224.laion2b
vit_huge_patch14_clip_224.laion2b
vit_huge_patch14_clip_224.laion2b_ft_in12k_in1k
vit_huge_patch14_clip_336.laion2b_ft_in12k_in1k
vit_large_patch14_clip_224.laion2b_ft_in12k_in1k
vit_large_patch14_clip_224.laion2b_ft_in1k
vit_large_patch14_clip_224.openai_ft_in12k
vit_large_patch14_clip_224.openai_ft_in1k
vit_large_patch14_clip_336.laion2b_ft_in1k

tf_efficientnetv2_l.in1k
tf_efficientnetv2_l.in21k_ft_in1k
tf_efficientnetv2_m.in21k
tf_efficientnetv2_s.in1k
tf_efficientnetv2_s.in21k_ft_in1k
tf_efficientnetv2_xl.in21k_ft_in1k
tf_mixnet_l.in1k
tf_mixnet_s.in1k
tf_mobilenetv3_large_100.in1k
tf_mobilenetv3_small_075.in1k
tf_mobilenetv3_small_minimal_100.in1k
tinynet_b.in1k
tinynet_d.in1k
tnt_s_patch16_224
twins_pcpvt_base
twins_pcpvt_small
twins_svt_large
vgg11
vgg13
vgg16
vgg19
visformer_small
vit_base_patch16_224.augreg_in1k
vit_base_patch16_224.augreg_in21k_ft_in1k
vit_base_patch16_224.orig_in21k_ft_in1k
vit_base_patch16_224_miil.in21k
vit_base_patch16_384.augreg_in1k
vit_base_patch16_384.orig_in21k_ft_in1k
vit_base_patch16_clip_224.laion2b_ft_in12k
vit_base_patch16_clip_224.laion2b_ft_in1k
vit_base_patch16_clip_224.openai_ft_in12k
vit_base_patch16_clip_224.openai_ft_in1k
vit_base_patch16_clip_384.laion2b_ft_in1k
vit_base_patch16_clip_384.openai_ft_in1k
vit_base_patch32_224.augreg_in1k
vit_base_patch32_224.augreg_in21k_ft_in1k
vit_base_patch32_384.augreg_in1k
vit_base_patch32_clip_224.laion2b
vit_base_patch32_clip_224.laion2b_ft_in1k
vit_base_patch32_clip_224.openai_ft_in1k
vit_base_patch32_clip_384.openai_ft_in12k_in1k
vit_base_patch8_224.augreg2_in21k_ft_in1k
vit_base_patch8_224.augreg_in21k_ft_in1k
vit_base_r50_s16_224.orig_in21k
vit_giant_patch14_clip_224.laion2b
vit_huge_patch14_224.orig_in21k
vit_huge_patch14_clip_224.laion2b_ft_in12k
vit_huge_patch14_clip_224.laion2b_ft_in1k
vit_large_patch14_clip_224.laion2b
vit_large_patch14_clip_224.laion2b_ft_in12k_in1k
vit_large_patch14_clip_224.openai
vit_large_patch14_clip_224.openai_ft_in12k_in1k
vit_large_patch14_clip_336.laion2b_ft_in12k_in1k
vit_large_patch14_clip_336.openai_ft_in12k_in1k

Unsupervised Embedding Quality Evaluation

| | |
|---|--|
| vit_large_patch16_224.augreg_in21k | vit_large_patch16_224.augreg_in21k_ft_in1k |
| vit_large_patch16_384.augreg_in21k_ft_in1k | vit_large_patch32_224.orig_in21k |
| vit_large_patch32_384.orig_in21k_ft_in1k | vit_large_r50_s32_224.augreg_in21k |
| vit_large_r50_s32_224.augreg_in21k_ft_in1k | vit_large_r50_s32_384.augreg_in21k_ft_in1k |
| vit_medium_patch16_gap_240.in12k | vit_medium_patch16_gap_256.in12k_ft_in1k |
| vit_medium_patch16_gap_384.in12k_ft_in1k | vit_relpos_base_patch16_224.sw_in1k |
| vit_relpos_base_patch16_cls_gap_224.sw_in1k | vit_relpos_base_patch32_plus_rpn_256.sw_in1k |
| vit_relpos_medium_patch16_224.sw_in1k | vit_relpos_medium_patch16_cls_224.sw_in1k |
| vit_relpos_medium_patch16_rpn_224.sw_in1k | vit_relpos_small_patch16_224.sw_in1k |
| vit_small_patch16_224.augreg_in1k | vit_small_patch16_224.augreg_in21k |
| vit_small_patch16_224.augreg_in21k_ft_in1k | vit_small_patch16_224.dino |
| vit_small_patch16_384.augreg_in1k | vit_small_patch16_384.augreg_in21k_ft_in1k |
| vit_small_patch32_224.augreg_in21k | vit_small_patch32_224.augreg_in21k_ft_in1k |
| vit_small_patch32_384.augreg_in21k_ft_in1k | vit_small_patch8_224.dino |
| vit_small_r26_s32_224.augreg_in21k | vit_small_r26_s32_224.augreg_in21k_ft_in1k |
| vit_small_r26_s32_384.augreg_in21k_ft_in1k | vit_srelpos_medium_patch16_224.sw_in1k |
| vit_srelpos_small_patch16_224.sw_in1k | vit_tiny_patch16_224.augreg_in21k |
| vit_tiny_patch16_224.augreg_in21k_ft_in1k | vit_tiny_patch16_384.augreg_in21k_ft_in1k |
| vit_tiny_r_s16_p8_224.augreg_in21k | vit_tiny_r_s16_p8_224.augreg_in21k_ft_in1k |
| vit_tiny_r_s16_p8_384.augreg_in21k_ft_in1k | volo_d1_224 |
| volo_d1_384 | volo_d2_224 |
| volo_d2_384 | volo_d3_224 |
| volo_d3_448 | volo_d4_224 |
| volo_d4_448 | volo_d5_224 |
| volo_d5_448 | volo_d5_512 |
| wide_resnet101_2.tv2_in1k | wide_resnet101_2.tv_in1k |
| wide_resnet50_2.racm_in1k | wide_resnet50_2.tv2_in1k |
| wide_resnet50_2.tv_in1k | xception |
| xception41 | xception41p |
| xception65 | xception65p |
| xception71 | xcit_large_24_p16_224 |
| xcit_large_24_p16_224_dist | xcit_large_24_p16_384_dist |
| xcit_large_24_p8_224 | xcit_large_24_p8_224_dist |
| xcit_large_24_p8_384_dist | xcit_medium_24_p16_224 |
| xcit_medium_24_p16_224_dist | xcit_medium_24_p16_384_dist |
| xcit_medium_24_p8_224 | xcit_medium_24_p8_224_dist |
| xcit_medium_24_p8_384_dist | xcit_nano_12_p16_224 |
| xcit_nano_12_p16_224_dist | xcit_nano_12_p16_384_dist |
| xcit_nano_12_p8_224 | xcit_nano_12_p8_224_dist |
| xcit_nano_12_p8_384_dist | xcit_small_12_p16_224 |
| xcit_small_12_p16_224_dist | xcit_small_12_p16_384_dist |
| xcit_small_12_p8_224 | xcit_small_12_p8_224_dist |
| xcit_small_12_p8_384_dist | xcit_small_24_p16_224 |
| xcit_small_24_p16_224_dist | xcit_small_24_p16_384_dist |
| xcit_small_24_p8_224 | xcit_small_24_p8_224_dist |
| xcit_small_24_p8_384_dist | xcit_tiny_12_p16_224 |
| xcit_tiny_12_p16_224_dist | xcit_tiny_12_p16_384_dist |
| xcit_tiny_12_p8_224 | xcit_tiny_12_p8_224_dist |
| xcit_tiny_12_p8_384_dist | xcit_tiny_24_p16_224 |
| xcit_tiny_24_p16_224_dist | xcit_tiny_24_p16_384_dist |
| xcit_tiny_24_p8_224 | xcit_tiny_24_p8_224_dist |
| xcit_tiny_24_p8_384_dist | |